CHEMISTRY OF MATERIALS
Article

Chem. Mater. **2009,** *21,* 2721–2726 2721
DOI:10.1021/cm9002417

Formation of Silicon Nanoporous Structures Induced by Colloidal Gold Nanoparticles in HF/H_2O_2 Solutions

Jianzhong Zhu,*[,†] Hilary Bart-Smith,[‡] Matthew R. Begley,[†,‡] Giovanni Zangari,[§] and Michael L. Reed[†]

[†]*Department of Electrical and Computer Engineering and* [‡]*Department of Mechanical and Aerospace Engineering and* [§]*Department of Materials Science and Engineering, University of Virginia, Charlottesville, Virginia 22904*

Received January 26, 2009. Revised Manuscript Received March 27, 2009

We developed an efficient method for the production of unique porous silicon structures, capable of achieving very small (less than 20 nm diameter) and uniform pore sizes, without the need for an external electrochemical cell or precoating of a discontinuous metal film. The method consists of the immersion of Si into a colloidal suspension of Au nanoparticles (NPs) containing a HF/H_2O_2 mixture. Gold colloids are known to be stable in neutral aqueous solutions, mainly because of the electrostatic repulsion between nanoparticles that carry the same negative surface charge. In acidic solutions obtained, for example, by addition of HF, however, conventional Au NPs colloids tend to lose their negative charge and to precipitate. A novel colloidal solution avoids NP precipitation upon acidification and thus enables Au NPs adsorption onto the Si surface, which triggers Si etching along definite crystallographic directions. The etching process occurs independently of the Si doping type or doping level. Because of its efficiency and simplicity, this method is of practical interest for the fabrication of submicrometer patterned silicon nanoporous structures. As a preliminary demonstration, the fabrication of Si membranes with nanosize pores is discussed.

Introduction

Porous silicon is a well-known, versatile material that has drawn a great deal of attention in applications such as optoelectronics,[1] photonic crystals,[2] optical filters,[3] membranes, and molecular sieves.[4,5] Porous silicon is usually synthesized by electrochemical anodization in HF-containing aqueous or organic solutions;[6−8] its morphology is determined by the anodization conditions, the electrolyte chemistry, as well as the Si doping type and the dopant concentration. Macro-, meso- and microporous structures (according to the IUPAC convention) are easily synthesized, but straight pores with narrow pore size distribution can be obtained only when the pores are wide (several 100 nm diameter) and under strictly controlled synthesis conditions.[9] Surface modification of silicon by the deposition of discontinuous metal films has been found to enable porous Si formation in suitable electrolytes without applying a potential; this process is usually called metal-assisted etching. The etching process is accelerated by the presence of the metal[10−13] and in some cases straight pores are formed.[14] The discontinuous metal films are deposited on the Si substrate by vacuum processes,[10] as well as by electro- or electroless plating.[14] Though very simple and efficient, this process suffers from two main drawbacks: it requires the previous deposition of a metal layer, and this process usually results in a wide size distribution of the deposited metal islands.[10−15] Consequently, the control of pore size is limited, and the lowest achievable dimensions are of the order of 50−100 nm. The addition of metal nanoparticles (NPs) to the etching solution followed by their adsorption onto the Si surface would overcome both these drawbacks: no previous deposition process would be needed, the range of achievable particle (and pore) sizes would be extended, and their size uniformity would be improved. In particular, strict control of the pore size could be achieved by utilizing, for example, commercially available colloidal gold. The major obstacle to this approach is

*To whom correspondence should be addressed. E-mail: jz8n@virginia.edu.

(1) Lehmann, V.; Gösele, U. *Appl. Phys. Lett.* **1991**, *58*, 856–858.
(2) Nicewarner-Peña, S. R.; Freeman, R. G.; Reiss, B. D.; He, L.; J. Peña, D.; Walton, I. D.; Cromer, R.; C. Keating, D.; Natan, M. J. *Science* **2001**, *294*, 137–141.
(3) Lehmann, V.; Ronnebeck, S. *Sens. Actuators, A* **2001**, *95*, 202–207.
(4) Fu, J.; Yoo, J.; Han, J. *Phys. Rev. Lett.* **2006**, *97*, 018103.
(5) Striemer, C. C.; Gaborski, T. R.; McGrath, J. L.; Fauchet, P. M. *Nature* **2007**, *445*, 749–753.
(6) Turner, D. R. *J. Electrochem. Soc.* **1958**, *105*, 402–408.
(7) Uhlir, A.Jr. *Bell Syst. Tech. J.* **1956**, *35*, 333–347.
(8) Smith, R. L.; Collins, S. D. *J. Appl. Phys.* **1992**, *71*, R1–R22.
(9) Föll, H.; Christophersen, M.; Carstensen, J.; Hasse, G. *Mater. Sci. Eng., R* **2002**, *39*, 93–141.
(10) Li, X.; Böhn, P. *Appl. Phys. Lett.* **2000**, *77*, 2572–2574.
(11) Peng, K.; Wu, Y.; Fang, H.; Zhong, X.; Xu, Y.; Zhu, J. *Angew. Chem., Int. Ed.* **2005**, *44*, 2737–2742.
(12) Asoh, H.; Arai, F.; Ono, S. *Electrochem. Commun.* **2007**, *9*, 535–539.
(13) Ono, S.; Oide, A.; Asoh, H. *Electrochim. Acta* **2007**, *52*, 2898–2904.
(14) Tsujino, K.; Matsumura, M. *Adv. Mater.* **2005**, *17*, 1045–1047.
(15) Hill, R. M. *Proc. R. Soc. London, Ser. A* **1969**, *309*, 397–417.

Published on Web 05/22/2009

the stabilization of the colloidal suspension in the etching solution.[16] Au colloidal suspensions in fact are stabilized in neutral solutions by the presence of a negatively charged citrate/acrylate coating, which is neutralized at low pH because of the shift in the citrate equilibrium 1 to the left

$$C_6H_8O_7 = C_6H_7O_7^- + H^+ \quad K_{eq} = 7.42 \times 10^{-4} \quad (1)$$

An acidic solution such as that utilized for porous Si formation would cause neutralization of the Au NPs capping layer, eventually inducing precipitation. In this paper, we show that a particular colloidal Au solution is relatively stable in HF solutions, enabling controlled NP adsorption even in low pH environments. As a consequence, this colloidal solution becomes a powerful tool for the synthesis of porous silicon. We find that this technique accelerates the etching rate of Si by 2 orders of magnitude, and simultaneously − similarly to other metal-induced pore formation methods − introduces anisotropy in the etching process, resulting in the preferential penetration of Au NPs along the ⟨100⟩ directions. The process does not require an external electrochemical cell or potentiostat and can thus be carried out without electrical leads and contacts.

Etching of silicon by immersion in HF/H_2O_2 solutions occurs very slowly, at a rate of about 1 nm/min.[17] Addition of H_2O_2 to an HF solution decreases the surface roughness of Si by rendering the etch process isotropic.[18] The presence of colloidal gold nanoparticles (MesoGold, nominal diameter 3.2 nm, measured by us to be in the order of 10 nm) in the HF/H_2O_2 solution (Au NPs-HF/H_2O_2), as we report here, results in a considerable enhancement of the silicon etching rate, up to approximately 100 nm/min. Additionally, the etching process in presence of the Au NPs is no longer isotropic. Finally, as described in the following, this procedure can be used to synthesize porous silicon structures with similar morphologies from Si wafers with different crystal orientations, as well as various doping types and concentrations.

Experimental Section

The Au NPs used in this study were MesoGold from Purest Colloids, Inc. (Westampton, NJ), with a purity of 99.99% and a nominal diameter of 3.2 ± 0.3 nm. The etching solution (Au NPs-HF/H_2O_2) was a 10:5:1 mixture (by volume) of 10 ppm colloidal Au NPs in deionized water, 30% H_2O_2, and 49% HF (the latter two supplied by Mallinckrodt Baker, Inc., Mallinckrodt, NJ). The as-prepared etchant is stable at room temperature for several months.

Etching experiments were carried out on 2 in. diameter silicon wafers with various doping types, doping concentrations and orientations, as summarized in Table S1 (see the Supporting Information). After sequential spin cleaning with trichloroethylene, isopropanol, and methanol, the samples were immersed into a polypropylene beaker containing the Au NPs-HF/H_2O_2 solution, at room temperature, and a magnetic stirrer. After a timed etch, the samples were rinsed with deionized water and dried with N_2 gas. Porous silicon regions formed on all silicon samples, as evidenced by scanning electron microscopy (SEM) images.

The adsorption characteristics from various colloidal Au solutions were determined by atomic force microscopy (AFM). All AFM images were obtained by using a Dimension 3100 instrument from Veeco Metrology Inc. (Santa Barbara, CA). To eliminate the noise in AFM images due to the possible surface roughening of Si after immersion in the etching solutions, we used cleaved muscovite mica from Ted Pella Inc. (Redding, CA) as the substrate, which is atomically flat. As-cleaved mica exhibits a negative surface charge at pH above 3.[19,20] To adsorb negatively charged Au NPs, we treated the mica surface with spermidine (Sigma-Aldrich, St Louis, MO), a polyamine that is positively charged in a wide range of pHs. Surface modification was achieved by placing a drop of 10 mM spermidine solution onto the new cleaved mica. After 5 min of incubation, the sample was rinsed with deionized water and then dried with N_2 gas. The spermidine-treated mica carries a positive surface charge, which attracts negatively charged nanoparticles. Both as-cleaved and modified mica substrates were utilized to determine the adsorption characteristics of Au NPs by placing a drop of the colloidal Au solution of choice onto the substrate.

Arrays of porous silicon regions were prepared by lithographically patterning a 2 in. Si wafer. After standard chemical cleaning, the Si sample was dipped into a buffered oxide etch (BOE) solution (Mallinckrodt Baker, Inc., Mallinckrodt, NJ) for a few seconds to strip the native oxide. A 600 nm SiO_2 layer was then thermally grown in wet O_2 at 1100 °C. The wafer was spin-coated with a 700 nm thick layer of AZ5206-E photoresist (AZ Electronic Materials, Somerville, NJ) and photolithographically patterned into a hexagonal array of 1.2 μm diameter circles. After a 2 min post bake on a 120 °C hot plate, the sample was etched in BOE for 12 min to transfer the patterns to the SiO_2 layer; the photoresist was subsequently stripped with acetone. Using the SiO_2 film as an etch mask, porous silicon regions were formed by immersing the sample into the Au NPs-HF/H_2O_2 solution for 5 min. The SiO_2 layer was finally stripped in BOE to reveal the ⟨100⟩-oriented nanochannel traces created by the Au NPs at the edges of the masked regions.

A model membrane with nanosized pores was fabricated by using this nanoparticle-assisted etching process. To this end, we used a double side polished p-type (001) Si as the starting material. First, a 600 nm thick SiO_2 layer, which served as etch mask, was thermally grown over the Si substrate in a H_2O/O_2 mixture at 1100 °C. At the front side of the silicon, the 600 nm thick SiO_2 acted as a protection layer against the successive etch process. The silicon thin membrane was microfabricated through selective etching from the back side in a 10% tetramethylammonium hydroxide (TMAH) solution (Aldrich Chemical Co, Milwaukee, WI), forming a truncated pyramidal shaped cavity. After the desired membrane thickness (about 5 μm) was reached, the sample was rinsed, then immersed into the Au NPs-HF/H_2O_2 solution. Au NPs adsorbed on the silicon

(16) Diegoli, S.; Mendes, P. M.; Baguley, E. R.; Leigh, S. J.; Iqbal, P.; Diaz, Y. R. G.; Begum, S.; Critchley, K.; Hammond, G. D.; Evans, S. D.; Attwood, D.; Jones, I. P.; Preece, J. A. *J. Exp. Nanosci.* **2006**, *1*, 333–353.
(17) Koynov, S.; Brandt, M. S.; Stutzmann, M. *Appl. Phys. Lett.* **2006**, *88*, 203107.
(18) Imou, N.; Ishiyama, T.; Omuraa, Y. *J. Electrochem. Soc.* **2006**, *153*, G59–66.
(19) Gaines, G. L.; Tabor, D. *Nature* **1956**, *178*, 1304–1305.
(20) Maslova, M. V.; Gerasimova, L. G.; Forsling, W. *Colloid J.* **2004**, *66*, 322–328.

film and penetrated into silicon along the ⟨100⟩ directions. During the experiment, the Au NPs-HF/H_2O_2 will also etch and dissolve the SiO_2 on the front side at a rate of about 50 nm/min. This may cause adsorption of Au NPs from the front side after a long time immersion. To avoid this, we transferred the sample to a HF/H_2O_2 solution without Au NPs after etching it in the Au NPs-HF/H_2O_2 solution for 5 min, such that no Au NP would be adsorbed from the front side of the silicon, whereas the Au NPs from the backside already present within the Si could continue to etch through the thin silicon film. After a timed etch, the sample was dipped in BOE for 10 min in order to strip all the residual oxide, rinsed with deionized water, dried with nitrogen gas, and imaged.

Results and Discussion

The scanning electron micrographs in Figure 1a−c show the temporal evolution (30, 60, 300 s etching, respectively) in the morphology of the porous silicon region formed by this method on a p-type (001) Si substrate. During the early etching phase, we observe pit formation at discrete locations. The etching paths increase in density and length until they cover the whole surface; a corresponding increase in surface roughness and depth of the porous silicon region results. In Figure 1d, a tilted (10°) cross-section reveals that the silicon has been converted to a porous region down to a depth of approximately 150 to 200 nm. Regression of the original surface from the initial level is limited to less than 10 nm, as demonstrated by the etching of patterned regions (see Figure S1 in the Supporting Information). Control experiments, using samples immersed in the HF/H_2O_2 etchant without Au NPs, do not result in the formation of any porous structures.

Porous silicon formation is thus critically dependent on the presence of Au NPs in solution. To better understand their influence on the etching process, we compared the adsorption properties of Au NPs from as-received solutions and from solutions acidified by the addition of HF. The as-received colloidal gold solution has a typical ruby red color as shown in Figure 2a (left). Addition of HF (overall concentration 3%) immediately changes the color of the colloidal gold solution to gray (Figure 2a, center); this hue decreases in intensity with time until, after a few hours, the solution becomes transparent (Figure 2a, right). AFM images b and c in in Figure 2 compare the adsorption of Au NPs from the as-received solution on as-cleaved and spermidine-treated mica, respectively. Au NPs with an average size of 14 nm were observed only on the spermidine-treated mica, which is positively charged, supporting the notion that the MesoGold colloidal NPs in the as-received solution are negatively charged. Adsorption of Au NPs from fresh (Figure 2a, center) and aged (Figure 2a, right) HF-acidified solutions was then carried out onto as-cleaved mica. The results are shown in d and e in Figure 2, respectively. In the former case, the adsorption of Au aggregates with larger size is observed; in the latter, a lower number density of smaller Au NPs is detected on the mica surface. These results suggest that acidification

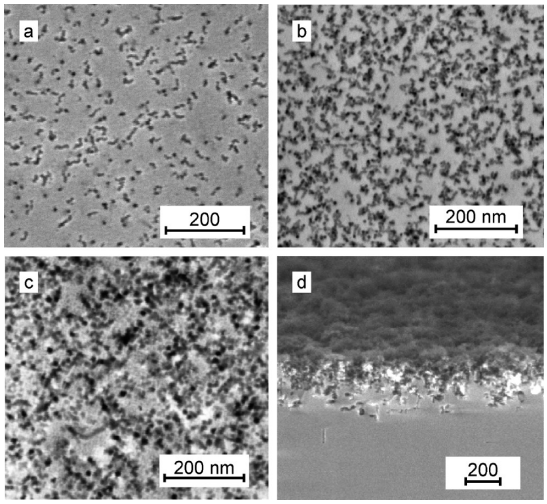

Figure 1. Scanning electron micrographs (SEM) of nanoporous network structures in p-type (001) silicon induced by colloidal gold nanoparticles (Au NPs) in an HF/H_2O_2 etchant. (a−c) Temporal evolution of the porous silicon formation process is evident: (a) 30 s etching, (b) 60 s etching, (c) 5 min etching. (d) Cross-sectional view (10° tilt) of the sample etched for 5 min, showing a porous silicon layer approximately 150−200 nm thick.

of the MesoGold colloidal gold solution induces neutralization and consequent aggregation of the Au NPs, which remain in suspension and can thus adsorb on the untreated mica surface. The change in color of the acidified solution also suggests that these aggregates eventually precipitate. A fraction of the colloidal gold however survives the aggregation process and remains in solution, as demonstrated by the smaller Au NPs adsorbed from the aged solution in Figure 2e. The Au NPs size distribution was determined from Figure 2e, and is presented in Figure S2 (see the Supporting Information). It is important to notice that the isoelectric points of both mica (pH 3−3.5)[21] and Si (pH 2)[22] are higher than the pH of the acidified solution (1.46). Under these circumstances, both mica and Si will exhibit a neutral or slightly positive surface charge, which will not hinder the adsorption of neutral Au NPs.

Similar adsorption experiments were conducted with two other gold colloids, one synthesized in our laboratory following the method of Turkevich et al.,[23] giving an average NPs diameter of about 50 nm, and the other commercially available from Ted Pella Inc. (Redding, CA), with NPs having an average diameter of 25 nm. In both cases, a few hours after acidification with HF, the Au NPs are observed to aggregate and completely precipitate from these solutions. As a consequence, Au NPs adsorption on as-cleaved or spermidine-treated mica surfaces from the latter solutions failed to occur. In addition, no nanoporous structures were observed upon

(21) Heyns, M. M.; Mertens, P. W.; Bearda, T.; Mertens, S.; Cornelissen, I.; Meuris, M.; De Gendt, S.; Nigam, T.; Degraeve, R.; Schaekers, M.; Groeseneken, G.; Teerlinck, I.; Kenens, C.; Vandervorst, W.; Knotter, D. M.; Vos, R.; Loewenstein, L. M.; Wolke, K. *IBM J. Res. Dev.* **1999**, *43*, 339–350.
(22) Ta, T. C.; Sykes, M. T.; McDermott, M. T. *Langmuir* **1998**, *14*, 2435–2443.
(23) Turkevich, J.; Stevenson, P. C.; Hillier, J. *Discuss. Faraday Soc.* **1951**, *11*, 55–75.

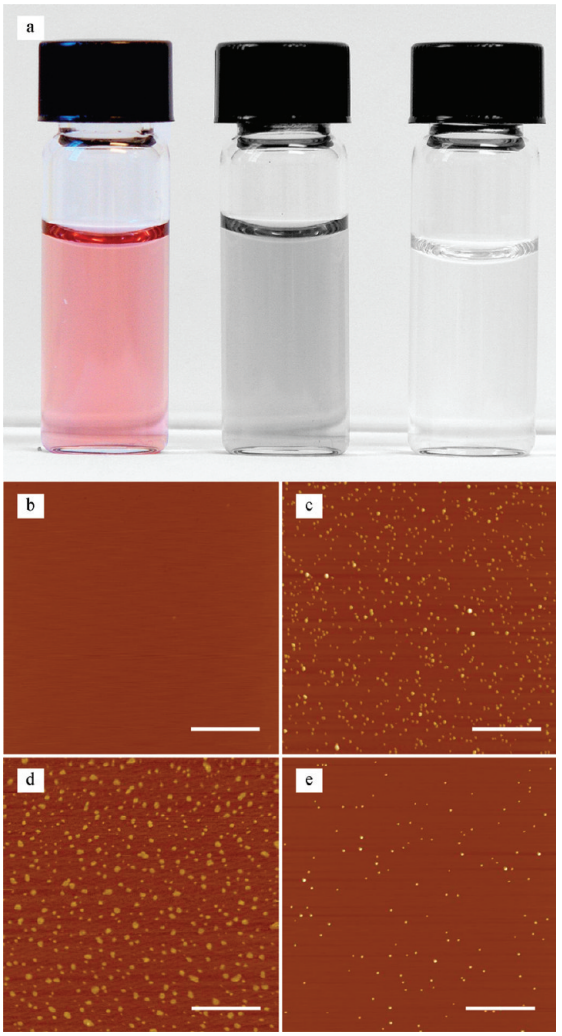

Figure 2. Colloidal Au NPs and their adsorption characteristics on muscovite mica. (a) Left, as-received MesoGold colloidal gold solution; center, same solution, immediately after addition of HF (final concentration 3%); right, MesoGold colloidal solution a few hours after acidification with HF. (b) AFM image of an as-cleaved mica surface after immersion in the solution at the left. No adsorption of Au NPs is observed. (c) AFM image of a spermidine-treated mica surface after immersion in the solution at left, showing a high density of Au NPs adsorbed on the surface. The Au NPs have a relatively narrow size distribution with a mean diameter of about 14 nm. (d) AFM image of an as-cleaved mica surface after immersion in the solution at center. Aggregates of Au NPs are adsorbed on the surface, suggesting a decrease in the repulsive interactions inhibiting Au NP adsorption in the neutral solution. (e) AFM image of an as-cleaved mica surface after immersion in the solution at right. Number density and mean size of the adsorbed Au NPs are slightly decreased. All AFM images are obtained in tapping mode. All scale bars represent 250 nm.

10 min immersion of Si wafers in HF/H_2O_2 solution containing either of the latter two Au NPs.

We believe that the failure to form porous Si in these instances is linked to the colloidal stability of the Au NPs in solutions of low pH. For the latter two solutions, the Coulombic repulsive interactions that stabilize the colloidal suspension at neutral pH[24] tend to decrease at lower pH because of the progressive neutralization of the capping layers, leading to NP precipitation.[25] On the other hand, the nature − or even the presence − of stabilizing coatings in MesoGold colloidal solutions is unknown; consequently, we cannot determine the mechanism responsible for the improved stability of the Au NPs in this latter case. The smaller size of the Au NPs in MesoGold could, however, contribute to their improved stability. The tendency for NP aggregation in fact is stronger in larger NP colloids, because the aggregation forces scale with the radius squared r^2 of the NPs.

The SEM images in Figure 1, in particular the rough correspondence between the width of the etch paths and the diameter of the adsorbed Au NPs, suggest that the etching process is induced by the Au NPs and results in the formation of channels excavated within the Si surface. To confirm this observation, we fabricated arrays of porous silicon circular regions by first patterning a Si surface using optical lithography. A hexagonal pattern of Si regions approximately 1.2 μm in diameter exposed to the electrolyte was defined onto a 600 nm thick thermally grown SiO_2 film. After a 300 s etch in the HF/H_2O_2 solution containing Au NPs, the oxide layer was stripped using a buffered HF solution. Examination of the surface, Figure 3, shows the resulting porous silicon regions. As depicted in Figure 3a, for p-type (001) Si, the edges of the etched circles are blurred, and reveal a network of channels extending outward from the pores, exclusively aligned along the [010] and [100] directions, both of which are in the plane of the (001) silicon surface. The pore size is about 16.7 ± 2.1 nm wide; the corresponding pore size distribution is shown in Figure S2 (see the Supporting Information). Notice how the pore size distribution traces the upper tail of the Au NPs size distribution.

We also observe that the nanometer sized channels in Figure 3a, which extend away from the edges of the porous silicon arrays, usually terminate with one of two different features. Bright end regions are indicated by black arrowheads, whereas dark end regions are indicated by white arrowheads. We hypothesize that the former features are Au NPs that have burrowed into the Si, forming ⟨100⟩-oriented channel, whereas the latter are vias through which the Au NPs escaped from or into the silicon surface after turning 90° away from the channel just formed, into another ⟨100⟩ direction. Energy-dispersive spectroscopy on etched Si surfaces (see Figure S3 in the Supporting Information) was unable to detect any Au signal. Although we have been unable to obtain direct evidence of the chemical nature of the bright features, the fact that only one bright or one dark spot is observed at the end of any single nanochannel, strongly suggests that the nanochannels are the result of penetration of Au NPs into the bulk Si.

Confirmation of the preferred penetration of the Au NPs along ⟨100⟩ was obtained by conducting experiments on Si wafers with other orientations. Figure 3b shows the result of etching a (011) oriented silicon substrate in the

(24) Diegoli, S.; Mendes, P. M.; Baguley, E. R.; Leigh, S. J.; Iqbal, P.; Garcia Diaz, Y. R.; Begum, S.; Critchley, K.; Hammond, G. D.; Evans, S. D.; Attwood, D.; Jones, I. P.; Preece, J. A. *J. Exp. Nanosci.* **2006**, *3*, 333–353.

(25) Woodruff, J. H.; Ratchford, J. B.; Goldthorpe, I. A.; McIntyre, P. C.; Chidsey, C. E. D. *Nano Lett.* **2007**, *7*, 1637–1642.

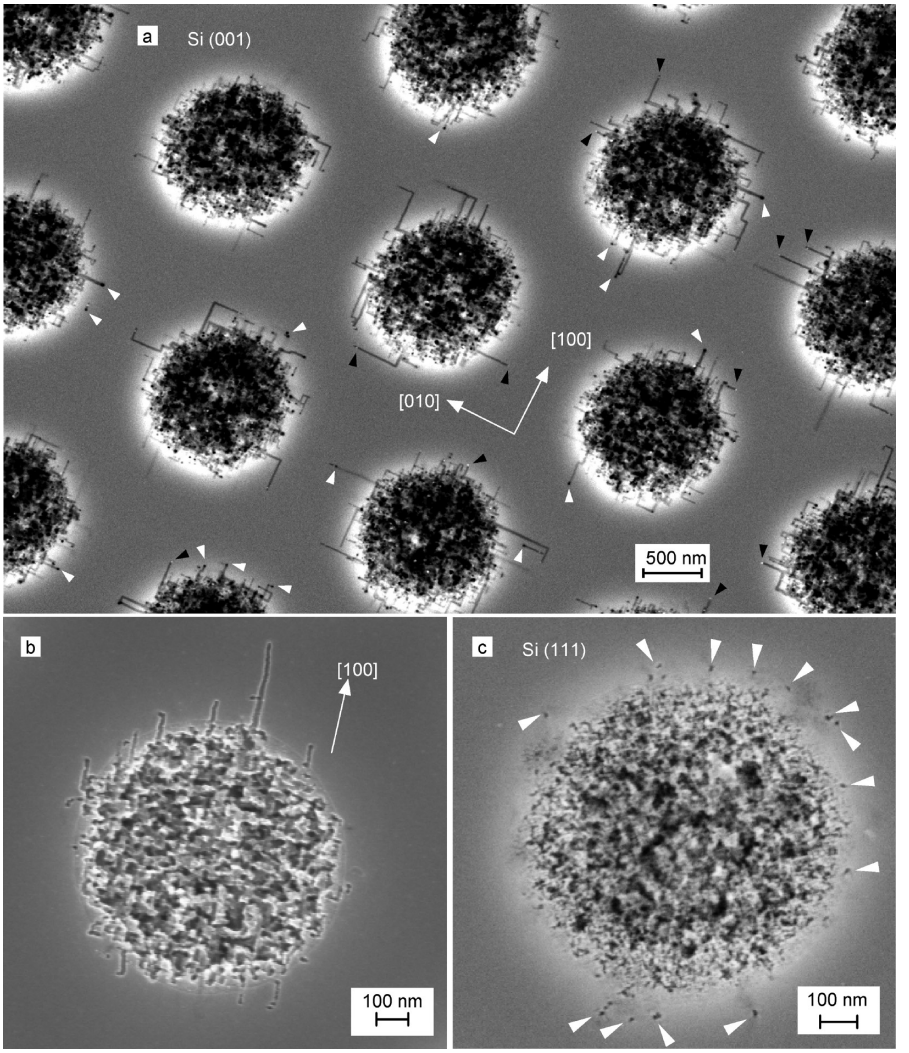

Figure 3. SEM of nanoporous Si arrays with different Si substrate orientations. Porous silicon patterns approximately 1.2 μm in diameter were fabricated by etching lithographically defined regions with HF/H_2O_2 solution containing Au NPs. (a) For a (001) Si substrate, at the periphery of the etched areas, numerous nanochannels extend away from the porous regions, always along the ⟨100⟩ directions. Two features are commonly observed at the ends of the nanochannels: bright areas, indicated by black arrowheads, and white areas, indicated by white arrowheads. (b) Nanochannels originating from the penetration of Au NPs into (011) Si are observed in one direction only, the single ⟨100⟩ direction lying in the (011) surface plane of the silicon. (c) No nanochannels extend from the periphery of porous Si regions in (111) Si, consistent with the absence of ⟨100⟩ directions lying in the (111) surface plane. However, we observe numerous nanometer-scale openings some distance away from the periphery; we interpret these as exit holes of nanochannels formed by localized dissolution along the ⟨100⟩ directions by Au NPs that have penetrated into the Si bulk.

Au NP-HF/H_2O_2 solution for 5 min; nanochannels resulting from the Au NP-induced etching process are oriented only in one direction, that of the single [100] direction that lies in the (011) surface plane. Figure 3c shows the result of an etching experiment using a (111) oriented Si substrate; in this case, no nanochannels are apparent on the wafer surface, consistent with the fact that no ⟨100⟩ directions lie in the (111) plane. On the other hand, we observe numerous etch pits about 20 nm in diameter (indicated by arrowheads in Figure 3c) near the periphery of the masked region, separated from the porous Si area. We interpret these as exit points of nanochannels formed by localized dissolution by the Au NPs in the bulk Si that have re-emerged after making a 90° turn into a different ⟨100⟩ direction. Similar results in terms of etching rate and porous morphology have been observed on Si substrates with different doping type (p-type and n-type) and various doping level, ranging from 2×10^{14} cm^{-3} to 1×10^{20} cm^{-3}, suggesting an independence of the etching process on Si conduction properties.

We hypothesize that the etching process is the combined result of the formation of local electrochemical cells at the silicon surface, originated by the adsorption of Au NPs, and of the presence of hydrogen peroxide. In this scenario, the H_2O_2 is reduced to water at the adsorbed Au NPs, by the following reaction[10,26] in acidic solution

$$H_2O_2 + 2H^+ + 2e^- \rightarrow 2H_2O$$

The availability of an oxidizing agent with a redox potential located at an energy lower than the valence band edge of Si (E^0 H_2O_2/H_2O = 1.763 V_{SHE}, corresponding to −6.263 eV, to be compared with the

(26) Shukla, A. K.; Raman, R. K. *Annu. Rev. Mater. Res.* **2003**, *33*, 155–68.

ionization energy of Si, −5.17 eV) makes it energetically favorable for electrons from silicon to participate in this reduction process. Furthermore, the Au NPs catalyze reduction of the oxidant without being dissolved in the solution, resulting in a more efficient reduction of hydrogen peroxide in the vicinity of the Au NPs. The migration of electrons at the Au NPs-Si contact also leaves behind compensating holes on the silicon surface, which are made available for silicon oxidation, through a reaction path that can be schematically summarized as[27−29]

$$Si + h^+_{VB} + 6F^- \rightarrow SiF_6^{2-} + 3e^-_{CB}$$

A large driving force for the pore etching process is provided by the availability of a redox couple in solution that is energetically located much below the valence band edge of Si; consequently, the reaction should occur independently of the details of the band bending configuration at immersed Si surfaces with different doping type and level, as indeed observed. In this way, the silicon atoms in the solid are dissolved into the etchant solution, mainly in the form of the soluble product SiF_6^{2-}.

The overall process is catalyzed by Au NPs and would thus proceed in their proximity; the formation of elongated channels may consequently be explained by the fact that the Au NPs tend to remain adsorbed at the Si surface that is being etched. The preference for the etched pores to grow along the ⟨001⟩ directions can be justified by the fact that {001} surfaces have the lowest number of Si−Si bonds and are thus more easily attacked, whereas {111} pore surfaces are passivated at a higher rate, thus favoring etching along the ⟨100⟩ directions. The {110} planes present an intermediate number of bonds and consequently an intermediate susceptibility to the etching process; the dissolution along the ⟨100⟩ direction should thus be preponderant. {110}[30] or {111}[31] surfaces in fact have been observed to form the walls of ⟨100⟩ oriented pores in electrochemically etched n-type and p-type Si. Similar arguments have been invoked by Föll et al. to support their Current Burst Model for porous Si formation.[31] Fluctuations in the kinetics of pore wall passivation would cause the observed occasional changes in the direction of the etching channel.

Preliminary experiments also demonstrated that nanosized pores could be formed in thin silicon membranes, generating model ultrafiltration membranes, by utilizing the property of the Au NPs in the HF/H_2O_2 solution to preferentially burrow into Si along the ⟨100⟩ directions. As shown in Figure 4d, Au NPs burrowed through a silicon membrane from the open window at the wafer backside and could be observed from the front side of the membrane. The pore pattern present on the front side

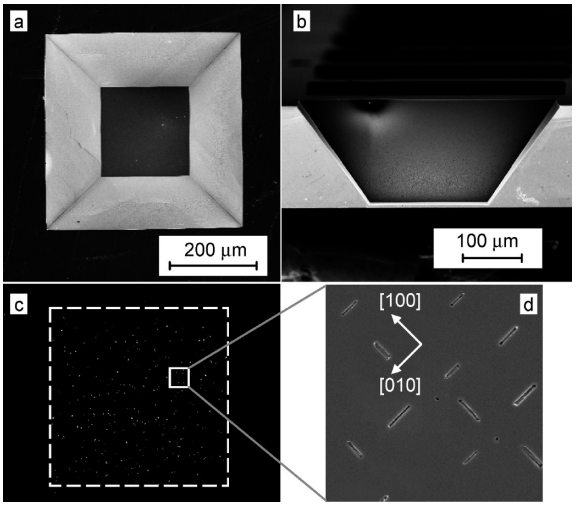

Figure 4. Fabrication of membranes with nanosized pores using colloidal gold nanoparticle-assisted etching. (a) SEM image of thin silicon membrane etched by TMAH (top view of the wafer backside). (b) Cross-sectional view of the membrane. (c) SEM image of the silicon membrane from the front side after etching in the Au NPs-HF/H_2O_2 solution, showing nanosized patterns within the membrane area. (d) High-magnification SEM image of the nanosized etch pits, displaying the penetration of Au NPs in the silicon membrane. Image size: $10 \times 10\ \mu m^2$.

of the silicon membrane is similar to those shown in Figure 3a, which indicates that the Au NPs were trapped at the backside Si-SiO_2 interface and carved the Si along the ⟨100⟩ directions. The dashed line rectangle in Figure 4c is exactly the same size as the bottom area of the window open from the backside, indicating that the through-holes are positioned within the thin Si region. The silicon wafer outside of this area is much thicker than the bottom membrane, hindering penetration of the Au NPs

Conclusions

We have demonstrated a simple and efficient method to synthesize unique porous silicon structures, capable of achieving very small (less than 20 nm) and uniform pore sizes, without the need for an external electrochemical cell or precoating of a discontinuous metal film. A novel colloidal gold solution, stable in acidic environment, was utilized to prepare an etchant containing Au NPs in a HF/H_2O_2 solution. By immersing a Si sample into this solution, random porous structures were formed in a shallow surface layer, while highly ordered nanopores along the ⟨100⟩ directions were created below this surface layer. Similar nanoporous structures were produced on a variety of Si substrates, regardless of crystal orientation, doping type, or doping level. This method may open up novel possibilities for the synthesis of controlled nanochannel networks in crystalline silicon, applicable for example to the fabrication of membranes for ultrafiltration or capillary electrophoresis.

Acknowledgment. This work was supported by the National Science Foundation, Award DMI 0507023.

Supporting Information Available: Additional figures and tables (PDF). This material is available free of charge via the Internet at http://pubs.acs.org.

(27) Zhang, X. G. *J. Electrochem. Soc.* **2004**, *151*, C69–C80.
(28) Kooij, E. S.; Vanmaekelbergh, D. *J. Electrochem. Soc.* **1997**, *144*, 1296–1301.
(29) Kolasinski, K. W. *Phys. Chem. Chem. Phys.* **2003**, *5*, 1270–1278.
(30) Searson, P. C.; Macaulay, J. M.; Ross, F. M. *J. Appl. Phys.* **1992**, *72*, 253–258.
(31) Jager, C.; Finkenberger, B.; Jager, W.; Christophersen, M.; Carstensen, J.; Foll, H. *Mater. Sci. Eng., B* **2000**, *69−70*, 199–204.